THE JOURNAL OF BIOLOGICAL CHEMISTRY
Vol. 276, No. 32, Issue of August 10, pp. 29632–29643, 2001

Printed in U.S.A.

Real-time Monitoring of the Interactions of Transforming Growth Factor-β (TGF-β) Isoforms with Latency-associated Protein and the Ectodomains of the TGF-β Type II and III Receptors Reveals Different Kinetic Models and Stoichiometries of Binding*

Received for publication, October 25, 2000, and in revised form, May 29, 2001
Published, JBC Papers in Press, May 29, 2001, DOI 10.1074/jbc.M009765200

Gregory De Crescenzo‡§, Suzanne Grothe‡, John Zwaagstra‡, Monica Tsang¶, and Maureen D. O'Connor-McCourt‡‖

From the ‡Biotechnology Research Institute (National Research Council Canada), Montreal, Quebec H4P 2R2, Canada and ¶R&D Systems, Minneapolis, Minnesota 55413

Mature transforming growth factor-β (TGF-β) is proteolytically derived from the C terminus of a precursor protein. Latency-associated protein (LAP), the N-terminal remnant of the TGF-β precursor, is able to bind and neutralize TGF-β. Mature TGF-β exerts its activity by binding and complexing members of two subfamilies of receptors, the type I and II receptors. In addition to these signaling receptors, TGF-β can also interact with an accessory receptor termed the type III receptor. Using a surface plasmon resonance-based biosensor (BIAcore), we determined the mechanisms of interaction of four binding proteins (LAP, the type II and III receptor ectodomains (EDs), and a type II receptor ED/Fc chimera) with three TGF-β isoforms, and we quantified their related kinetic parameters. Using global fitting based on a numerical integration data analysis method, we demonstrated that LAP and the type II receptor/Fc chimera interacted with the TGF-β isoforms with a 1:1 stoichiometry. In contrast, the type II ED interactions with TGF-β were best fit by a kinetic model assuming the presence of two independent binding sites on the ligand molecule. We also showed that the type III ED bound two TGF-β molecules. Further experiments revealed that LAP was able to block the interactions of TGF-β with the two EDs, but that the two EDs did not compete or cooperate with each other. Together, these results strongly support the existence of a cell-surface complex consisting of one type III receptor, two TGF-β molecules, and four type II receptors, prior to the recruitment of the type I receptor for signal transduction. Additionally, our results indicate that the apparent dissociation rate constants are more predictive of the neutralizing potency of these TGF-β-binding proteins (LAP, the type II and III receptor EDs, and the type II receptor/Fc chimera) than the apparent equilibrium constants.

Transforming growth factor-β (TGF-β)[1] belongs to a family of peptides involved in the regulation of growth, development, tissue repair, tumorigenesis, inflammation, and host defense (1–4). Three isoforms (termed TGF-β1, TGF-β2, and TGF-β3) are present in mammalian cells. Mature TGF-β isoforms correspond to the carboxyl-terminal domain of a precursor protein termed prepro-TGF-β. Cleavage by a proconvertase yields both mature TGF-β and a prodomain called the latency-associated protein (LAP). Both TGF-β and LAP are disulfide-bonded homodimers and have been shown to remain noncovalently associated with each other after cleavage (5). This complex is inactive (latent), as it is not recognized by the TGF-β signaling receptors.

Mature TGF-β signals by binding and complexing two receptors, the type I and II receptors (6). Once this heteromeric receptor·ligand complex is formed, the type II receptor phosphorylates the type I receptor, and the signal is then translocated to the nucleus by members of the SMAD family (7, 8). In addition to the signaling receptors, TGF-β can also interact with a receptor known as the type III receptor that apparently does not signal. This receptor is thought to act as an enhancer of TGF-β activity by promoting its access to the signaling receptors (especially for the TGF-β2 isoform, which has a low affinity for the type II receptor) (9, 10). The type III receptor possesses two ligand-binding domains, one located in the N-terminal region and one in the C-terminal region of its ectodomain (11–14). However, it remains unclear if one or two TGF-β molecules bind to the type III receptor. The isolated ectodomains (EDs) of the type II and III receptors are soluble and retain their ability to bind to TGF-β isoforms (15–17). They exert, similarly to LAP, an antagonistic activity by binding to TGF-β and sequestering it away from cell-surface receptors (15, 18).

The purpose of this study was to determine the binding mechanisms of these three proteins, LAP and the type II and III EDs, in addition to a type II receptor ectodomain/Fc chimera with the three mammalian TGF-β isoforms. To quantify the kinetic parameters of these interactions, we used the BIAcore, a surface plasmon resonance-based biosensor that allows real-time measurement of macromolecular interactions. We demonstrated the following. 1) LAP interacts with all the TGF-β isoforms according to a conformational change model and a 1:1 stoichiometry. 2) TGF-β1 and TGF-β3 interactions with the type II ED are best fit by a kinetic model assuming the presence of two independent binding sites on the ligand molecule for the type II ED. In contrast, the interactions of these TGF-β isoforms with a type II ED/Fc chimera are best depicted by a rearrangement model and a 1:1 stoichiometry. 3) The type III

* The costs of publication of this article were defrayed in part by the payment of page charges. This article must therefore be hereby marked "*advertisement*" in accordance with 18 U.S.C. Section 1734 solely to indicate this fact.

§ Supported by the Protein Engineering Network of Centers of Excellence.

‖ To whom correspondence should be addressed: Biotechnology Research Inst. (NRC), 6100 RoyalMount Ave., Montreal, Quebec H4P 2R2, Canada. Tel.: 514-496-6382; Fax: 514-496-5143; E-mail: maureen.o'connor@nrc.ca.

[1] The abbreviations used are: TGF-β, transforming growth factor-β; LAP, latency-associated protein; ED, ectodomain; RU, resonance unit(s).

ED binds two TGF-β molecules. 4) LAP is able to block the interactions of TGF-β with the two ectodomains. 5) Both ectodomains do not compete or cooperate with each other when binding to TGF-β. Finally, the ability of LAP, the type II ED, the type II ED/Fc chimera, and the type III ED to antagonize binding of TGF-β to its cell-surface receptors was tested using mink lung epithelial cells stably transfected with a TGF-β-sensitive luciferase reporter gene. These results were correlated with the BIAcore data.

The present analyses strongly support the existence of a complex consisting of one type III receptor, two TGF-β molecules, and four type II receptors within the signaling receptor complex. Additionally, results of our kinetic analysis indicate that the apparent dissociation rate constant may be the best predictor of the antagonistic potency of TGF-β-binding proteins.

EXPERIMENTAL PROCEDURES

Equipment and Reagents

The BIAcore 1000, CM5 sensor chips, *N*-hydroxysuccinimide, *N*-ethyl-*N*′-(3-diethylaminopropyl)carbodiimide hydrochloride, and 1 M ethanolamine (pH 8.5) were purchased from BIAcore Inc. (Piscataway, NJ). Recombinant TGF-β isoforms (human recombinant TGF-β1, TGF-β2, and TGF-β3 expressed in Chinese hamster ovary, NSO, and Sf21 cells, respectively), recombinant β1-LAP (expressed in Chinese hamster ovary cells), and the recombinant extracellular domains of the TGF-β type II and III receptors in addition to the TGF-β type II receptor/Fc chimera corresponding to the 159 amino acid residues of the type II ED fused to the Fc region of human IgG_1 (all expressed in NSO cells) were provided by R&D Systems (Minneapolis, MN).

Surface Plasmon Resonance Experiments

Immobilization of TGF-β on Sensor Chips—TGF-β isoforms were coupled to CM5 sensor chip surfaces using the standard amine coupling procedure and a flow rate set at 5 μl/min. Sequential injections consisted of a 0.05 M *N*-hydroxysuccinimide and 0.2 M *N*-ethyl-*N*′-(3-diethylaminopropyl)carbodiimide hydrochloride mixture (35 μl) followed by TGF-β solutions (0.8–1.6 μg/ml) in 10 mM acetic acid (pH 4.0) until the desired amount of coupled TGF-β was reached. A solution of 0.1 M ethanolamine HCl (35 μl, pH 8.5) was then used to block the remaining activated carboxyl groups. Control dextran surfaces were also generated by replacing the TGF-β solutions with running buffer (20 mM Hepes (pH 7.4), 150 mM NaCl, 3.4 mM EDTA, and 0.05% Tween 20).

Kinetic Assays on the BIAcore—All the kinetic experiments were carried out at 25 °C at a flow rate of 5 μl/min, except for the mass transport experiments, for which different injections of each analyte (human LAP, the type II ED, the type II ED/Fc chimera, and the type III ED) were performed at flow rates ranging from 5 to 30 μl/min. Running buffer was used for diluting all the species that were injected over the TGF-β isoform surfaces. Different concentrations of LAP (73 kDa), the type II ED (27 kDa), the type II ED/Fc chimera (120 kDa), and the type III ED (112.5 kDa) were injected over various TGF-β (25 kDa) surfaces as well as over a control surface for 300 s, following which the analyte solutions were replaced by buffer for 300 s. Regeneration of the sensor chip for subsequent injections was accomplished by two pulses of HCl (20 mM, 120 s), followed by an EXTRACLEAN procedure done according to the BIAcore manual.

Data Preparation and Analysis—Sensorgrams were prepared and globally fit using nonlinear least-squares analysis and numerical integration of the differential rate equations using the SP*Revolution*® software package. The data preparation was done mainly as described elsewhere (19). Briefly, each sensorgram generated using a control surface was subtracted from the corresponding experimental sensorgrams, and the resulting curves were transformed to concentration units using the molecular mass of the injected species, the equivalence of 1000 resonance units (RU) per 1 ng/mm^2, and a matrix thickness of 100 nm. Each data set (which consists of sensorgrams from injections of different analyte concentrations over the same surface) was then analyzed using several different kinetic models that are available in the SP*Revolution*® software.

Mathematic Modeling and Parameter Estimation—In SP*Revolution*®, the various kinetic models were transposed into differential equations by making a mass balance on all species present in the dextran matrix. These sets of nonlinear differential equations were solved numerically using an adaptive step-size Runge-Kutta method (20). The resulting routine was used in a nonlinear regression program using Marquardt's algorithm (21) to estimate the values of the constants from experimental data. The schematic representation of the models used for the data analysis and their related sets of differential rate equations are listed in Table I. For each model, the kinetic parameters as well as the active quantity of ligand immobilized on the matrix were considered as global parameters for a given set of curves. Moreover, two local parameters were added for each curve to take into account the refractive index changes at the beginning of the wash-on and wash-off phases.

Evaluation of the Quality of the Fit for the Various Kinetic Models—For each set of residuals, three statistical values were calculated. The first statistical value is the S.D. of the residuals. The second statistical value is the "+ or − sign" statistic (Z_1) (22). Each residual is replaced by its sign value (+ or −), and the following statistic is then calculated on the newly created data set, $Z_1 = (n \times (R_1 - 1) - 2 \times n_1 \times n_2)/(2 \times n_1 \times n_2(2 \times n_1 \times n_2 - n)/(n - 1))^{1/2}$, where R_1 is the number of positive runs, n_1 is the + number, and n_2 is the − number. The third statistical value is the "run up and down" statistic (Z_2) (22). Using the residual set $x(i)$, a new set of data, y, is created with $y(i) = x(i) - x(i + 1)$. As for the above test, each y value is then replaced by its sign value (+ or −). If we call R_2 the number of positive $y(i)$ of the runs, then the statistic Z_2 equals $(R_2 - ((2 \times n - 1)/3))/((16 \times n - 29)/90)^{1/2}$. Assuming that the residuals are independent, the Z_1 and Z_2 statistics follow a normal law with a mean equal to 0 and a variance equal to 1.

BIAcore Multiple Binding Experiments—The effect of pre-binding of LAP was assayed as follows. 300-s injections of LAP solutions (ranging in concentration from 0 to 200 nM in the case of TGF-β1 or from 0 to 400 nM for TGF-β2 and TGF-β3) were performed over TGF-β isoform surfaces (155, 250, and 250 RU of coupled TGF-β1, TGF-β2, and TGF-β3, respectively) and a control surface. All injections were followed by a short wash-off phase (100 s) and a 300-s injection of the type II or III ED at a fixed concentration of 400 or 600 nM, respectively. The quantity of each ectodomain bound after 300 s was expressed as a percentage of binding after 300 s in the absence of LAP. This was plotted against the amount of LAP pre-bound to the surface, which was expressed as the percentage of maximum LAP binding and was determined by a numerical integration approach (using a rearrangement model).

The effect of pre-binding of the type II and III EDs was assayed as follows. Injections of the type III ED (0–800 nM, 300 s) were followed by 300-s co-injections of a mixture of the type III ED (at the same concentration as for the first injection) and the type II ED at 500 nM. The reverse experiment was also carried out. The results were expressed as percent binding of the ectodomain that was injected second, and this was plotted against the concentration of the ectodomain injected first.

Testing the Antagonistic Inhibitor Potency of the Type II and III EDs and LAP Using a Luciferase Assay in Mink Lung Epithelial Cells

Mink lung epithelial cells stably transfected with the *PAI-1* promoter fused to the firefly luciferase reporter gene were a generous gift of Dr. D. Rifkin (23). These cells were plated in 96-well tissue culture plates (2×10^4 cells/well) in Dulbecco's modified Eagle's medium containing 5% fetal bovine serum and were allowed to attach for at least 3 h at 37 °C in a 5% CO_2 atmosphere. Cells were then washed with PBS, and the medium was replaced by Dulbecco's modified Eagle's medium containing 1% fetal bovine serum and 0.1% bovine serum albumin. TGF-β isoforms (10 pM) and LAP, the type II ED, the type II ED/Fc chimera, or the type III ED at various concentrations were then added. After an overnight incubation, the medium was removed, and the cells were washed twice with PBS. Cells were then lysed and assayed for luciferase activity using the Promega luciferase assay kit according to the manufacturer's instructions. Luminescence was measured with a Berthold Lumat LB9501 luminometer. The activity was expressed as the percentage of the activity of each TGF-β isoform in the absence of LAP, the type II ED, the type II ED/Fc chimera, or the type III ED.

RESULTS

BIAcore Analysis of TGF-β Interactions with LAP, the Type II ED, the Type II ED/Fc Chimera, and the Type III ED—The first goal of our study was to determine the kinetic mechanisms and kinetic constants related to the interactions of three mammalian TGF-β isoforms with four different proteins: TGF-β1 LAP and type II and III EDs, in addition to an artificially dimerized type II ED (the type II ED/Fc chimera). In a typical BIAcore experiment, one of the binding partners is immobilized

on the sensor chip surface (called the ligand in BIAcore terminology). A solution containing the other binding partner is injected over the sensor chip surface (called the analyte in BIAcore terminology). The mass accumulation of the analyte on the surface as it binds to the ligand is recorded in arbitrary resonance units, which vary with the refractive index of the interfacing medium. As the change in the refractive index is a linear function of the surface concentration of the macromolecules, the RU signal is proportional to the mass accumulation of the analyte. This constitutes the wash-on phase of the experiment. After a certain period of time, the analyte solution is replaced by buffer, and the dissociation of surface complexes is monitored (the wash-off phase). Since the wash-on and wash-off phases of the curve (sensorgram) are recorded in real time, it is possible to derive kinetic parameters from these sensorgrams.

In preliminary experiments, injection of TGF-β1 over a control dextran surface (no ligand immobilized) resulted in a significant increase in the surface plasmon resonance signal with time, indicating that TGF-β1 binds nonspecifically to the dextran surface. In contrast, no interaction was detectable when LAP, the type II ED, the type II ED/Fc chimera, and the type III ED were injected over the control surface (data not shown). Therefore, we immobilized the TGF-β isoforms on the sensor chip and injected LAP, the type II ED, the type II ED/Fc chimera, or the type III ED over the surface.

In preliminary experiments using TGF-β-coupled surfaces with LAP, type II ED, type II ED/Fc chimera, or type III ED flowing, the binding data were fit using nonlinear least-squares analysis and numerical integration of the differential rate equations corresponding to a simple kinetic model. This model did not yield a good fit as judged by the non-random distribution in the residuals (the difference between calculated and experimental data) (data not shown). This deviation from a simple one-to-one interaction model may result from the existence of a more complex biological interaction. Alternatively, it may be due to the presence of artifacts such as mass transport and rebinding effects or steric hindrance/crowding problems (24) that can occur when the BIAcore experimental conditions are not optimized. To minimize these artifacts and to perform kinetic studies, we generated different surfaces where low quantities of TGF-β isoforms were coupled (from 50 to 700 RU). This approach reduces so-called crowding problems by minimizing the masking of potential ligand-binding sites on the surface by accumulated ligand·analyte complexes. Additionally, it reduces mass transport and rebinding artifacts that occur if the transportation rate of the analyte through the unstirred layer over the surface is slow compared with the kinetics of binding.

Based on the results from these preliminary experiments, we coupled the minimum amount of each TGF-β isoform required to obtain an acceptable signal-to-noise ratio when injecting LAP, the type II ED, the type II ED/Fc chimera, or the type III ED. Due to the different apparent kinetics and affinities of these binding proteins for TGF-β, it was necessary to use surfaces with different amounts of coupled TGF-β for each interaction. For each TGF-β isoform surface, the absence of mass transport limitation and/or rebinding artifacts was tested by injecting the lowest concentration of the analyte used in the kinetic study at different flow rates ranging from 5 to 30 μl/min. Since the sensorgrams were superimposable when varying the flow (data not shown), it can be concluded that the diffusion of the analyte from the bulk flow to the matrix is not kinetically limiting under these flow and surface conditions.

We next injected LAP, type II ED, type II ED/Fc chimera, and type III ED solutions ranging in concentration from 12.5 to 200, 32 to 355, 18 to 500, and 50 to 800 nM, respectively, over the TGF-β1, TGF-β2, and TGF-β3 surfaces that were optimized for each binding partner. The sensorgrams corresponding to the experiments using TGF-β3 surfaces are shown in Figs. 1–4. Similar sensorgrams were observed for the TGF-β1 and TGF-β2 surfaces (data not shown). Each set of sensorgrams was analyzed by curve fitting using the SP*Revolution*® software package (19, 25). This method of data analysis has been shown to be critical for distinguishing between different binding models and determining kinetic constants that are consistent with all the time points in all the sensorgrams in one set (26–28). In all cases, we observed a poor fit when using a simple one-to-one model to depict the interactions (Figs. 1–4, *panels C*; and data not shown). Since artifacts such as mass transport limitation and rebinding and crowding problems were already eliminated or minimized, we tested if such deviations from fitting a simple model could be due to more complex interaction mechanisms.

We tested three more complex kinetic models for each TGF-β-binding protein/TGF-β data set. The selection of these more complex models was based on their potential biological relevance (see "Discussion" for literature references to these mod-

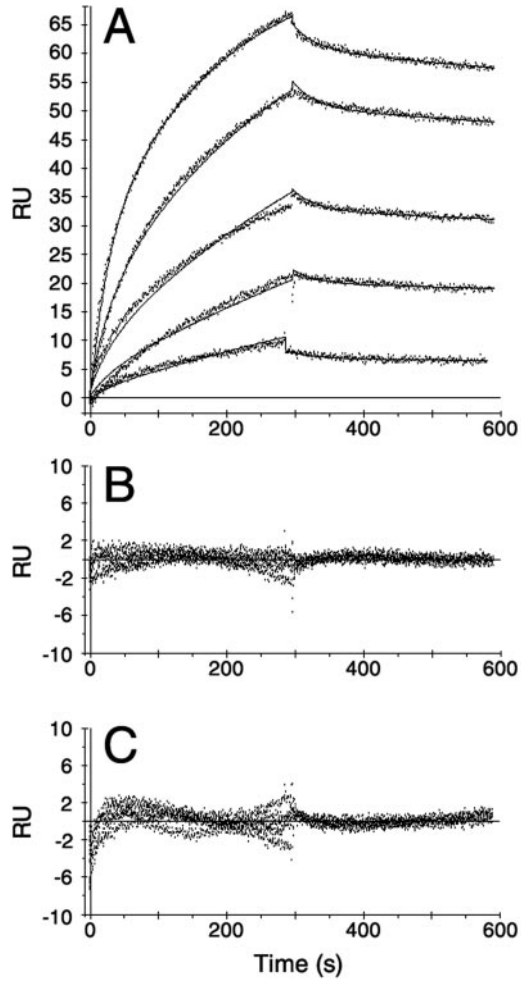

FIG. 1. **Global analysis of the LAP interaction with the TGF-β3 isoform.** *A*, global fit of the LAP/TGF-β3 interaction sensorgrams. Different concentrations of LAP ranging from 12.5 to 200 nM were injected over 150 RU of immobilized TGF-β3 and over a control dextran surface. The *points* are the resonance units obtained after blank subtraction, and the *solid lines* represent the fit when integrating all the curves simultaneously using a rearrangement model. *B*, residuals from the fit of the LAP/TGF-β3 interaction using the rearrangement model. *C*, residuals from the fit of the LAP/TGF-β3 interaction using a simple one-to-one model.

TABLE I

Schematic representation of the kinetic models and the related differential equations

L and A correspond to the ligand and the analyte, respectively. L_1 and L_2 stand for two sites that are present on the same molecule of ligand (L) and are able to bind analyte independently. L_iA is used when a molecule of analyte is already bound to the *i*th site of the ligand. LA* and LA stand for a complex composed of one molecule of ligand and analyte in a rearranged or initial form, respectively. Finally, ALA and LAL depict complexes composed of one ligand and two analyte molecules or vice versa.

Simple one-to-one interaction $L + A \leftrightarrow LA$	$\frac{d[L]}{dt} = -k_a[L][A] + k_d[LA]; \frac{d[LA]}{dt} = k_a[L][A] - k_d[LA]$
Two independent sites on ligand $L_1 + A \leftrightarrow L_1A$	$\frac{d[L_1]}{dt} = -k_{a1}[L_1][A] + k_{d1}[L_1A]; \frac{d[L_2]}{dt} = -k_{a2}[L_2][A] + k_{d2}[L_2A]; \frac{d[L_1A]}{dt} = k_{a1}[L_1][A] - k_{d1}[L_1A]; \frac{d[L_2A]}{dt} = k_{a2}[L_2][A] - k_{d2}[L_2A]$
$L_2 + A \leftrightarrow L_2A$ $L_1A + A \leftrightarrow ALA$ $L_2A + A \leftrightarrow ALA$	
Rearrangement of complex $L + A \leftrightarrow LA \leftrightarrow LA^*$	$\frac{d[L]}{dt} = -k_{a1}[L][A] + k_{d1}[LA]; \frac{d[LA^*]}{dt} = k_{a2}[LA] - k_{d2}[LA^*]; \frac{d[LA]}{dt} = k_{a1}[L][A] - k_{d1}[LA] + k_{d2}[LA^*] - k_{a2}[LA]$
Two sites on analyte (avidity) $L + A \leftrightarrow LA$	$\frac{d[L]}{dt} = -k_{a1}[L][A] + k_{d2}[LA] + k_{d2}[LAL] - k_{a2}[LA][L]; \frac{d[LA]}{dt} = k_{a1}[L][A] - k_{d1}[LA] + k_{d2}[LAL] - k_{a2}[LA][L]; \frac{d[LAL]}{dt} = k_{a2}[LA][L] - k_{d2}[LAL]$
and then $LA + L \leftrightarrow LAL$	

els). These models included 1) a model depicting the occurrence of a rearrangement in the TGF-β-binding protein·TGF-β complex; 2) a model assuming the presence of two independent binding sites on the TGF-β molecule (two-sited ligand model); and 3) a model depicting the presence of two distinct binding sites on the injected binding protein (this can also be termed an avidity model since it involves the binding of a bivalent analyte to a fixed ligand). The schematic representations of the models and their respective differential rate equations are shown in Table I. The residual plots, the S.D. of the residuals, as well as the Z_1 and Z_2 statistics can be used to judge the adequacy of the models when tested against the same data set. That is, when a kinetic model adequately depicts a biomolecular interaction, the residuals will be minimal and randomly distributed around a zero value. More specifically, a significantly large amplitude of the residuals, long series of positive or negative points, or long series of ascending or descending points will be absent from the residual plot. These characteristics will be reflected in low values for the S.D., the Z_1 statistic, and the Z_2 statistic, respectively.

Based on this type of analysis, it was observed that the LAP interaction with TGF-β3 was best fit by a rearrangement model (Fig. 1, *A* and *B*; and Table II). The same conclusion was made for TGF-β1 and TGF-β2 binding to LAP (data not shown). An analysis of the type II ED injections over TGF-β3 indicated that this interaction was best fit by the two-sited ligand model (Fig. 2, *A* and *B*; and Table II). The same model was determined to be the most adequate for the type II ED/TGF-β1 interaction (data not shown). No interaction was detected between the TGF-β2 isoform and the type II ED, which is consistent with our previous results (29). A model assuming the presence of two binding sites on the type III ED (avidity model) gave the best fit for the TGF-β3 isoform (Fig. 3, *A* and *B*; and Table II) and the TGF-β1 isoform (data not shown). In the case of the TGF-β2 isoform interacting with the type III ED, the fit was relatively good, but essentially the same for the rearrangement and the two-sited analyte (avidity) models (data not shown). Finally, in the case of the type II ED/Fc chimera, the TGF-β3 isoform interaction was best fit by a rearrangement model (Fig. 4, *A* and *B*; and Table II). The same model was found to be the best for the TGF-β1 isoform.

To confirm the stoichiometries of binding that were determined above using the different surfaces that were optimized for each binding partner/TGF-β isoform interaction and to provide an additional test for internal self-consistency, we next injected the LAP and type II and III ED binding proteins over the same TGF-β1 surface (125 RU immobilized). Once again, the rearrangement, two-sited ligand, and avidity models best described the interaction of TGF-β1 with LAP and the type II and III EDs, respectively (Fig. 5, *A–C*, respectively). The same comparison could not be carried out on a TGF-β2 surface since the type II ED does not detectably bind TGF-β2. Also, a TGF-β3 surface could not be used for a similar experiment due to the differences in the apparent affinities of the three binding proteins for this isoform (*i.e.* it was impossible to eliminate non-biological artifacts at the same time as obtaining a sufficient signal for all three binding proteins on one TGF-β3 surface). Since the three binding proteins were analyzed on the same TGF-β1 surface, the quantity of immobilized active TGF-β1 that is determined by curve fitting as a global parameter (*i.e.* one value is calculated for each set of curves) should be the same for all tested binding proteins if the kinetic models are relevant. As shown in Table III, the rearrangement, two-sited

TABLE II

S.D. of the residuals and Z_1 and Z_2 statistics for the interaction of TGF-β3 with LAP, the type II and III EDs, and the type II ED/Fc chimera as calculated from the data shown in Figs. 1–4 using four kinetic models

The best fitting kinetic model is indicated in boldface type. These results are representative of at least three experiments.

Interaction	Kinetic model			
	Simple	Two-sited ligand	Rearrangement	Two-sited analyte (avidity)
LAP/TGF-β3				
S.D.	1.004	0.920	**0.670**	0.900
$Z1$	32.06	29.06	**23.32**	29.69
$Z2$	1.630	1.670	**1.550**	1.630
Type II ED/TGF-β3				
S.D.	5.197	**1.620**	2.900	5.710
Z_1	35.88	**20.12**	32.40	38.97
Z_2	4.750	**1.613**	2.151	5.110
Type III ED/TGF-β3				
S.D.	1.943	0.860	0.850	**0.689**
Z_1	47.43	28.28	27.29	**21.95**
Z_2	1.087	0.160	0.300	**0.150**
Type II ED/Fc chimera/TGF-β3				
S.D.	3.020	1.213	**0.966**	1.146
Z_1	28.97	18.33	**16.32**	17.36
Z_2	2.704	2.800	**2.704**	3.000

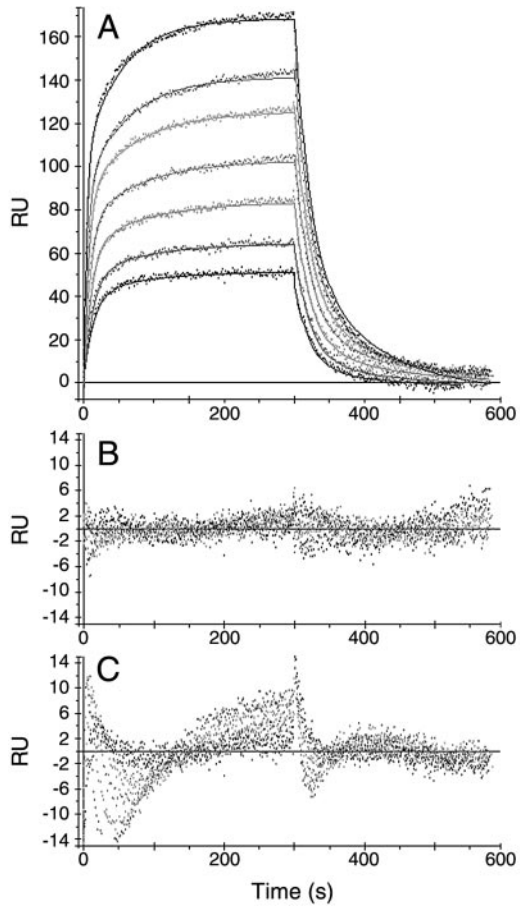

FIG. 2. **Global analysis of the type II ED interaction with the TGF-β3 isoform.** *A*, global fit of the type II ED/TGF-β3 interaction sensorgrams. Different concentrations of the type II ED ranging from 32 to 355 nM were injected over 700 RU of immobilized TGF-β3 and over a control dextran surface. The *points* are the resonance units obtained after blank subtraction, and the *solid lines* represent the fit when integrating all the curves simultaneously using a two-sited ligand model. *B*, residuals from the fit of the type II ED/TGF-β3 interaction using the two-sited ligand model. *C*, residuals from the fit of the type II ED/TGF-β3 interaction using a simple one-to-one model.

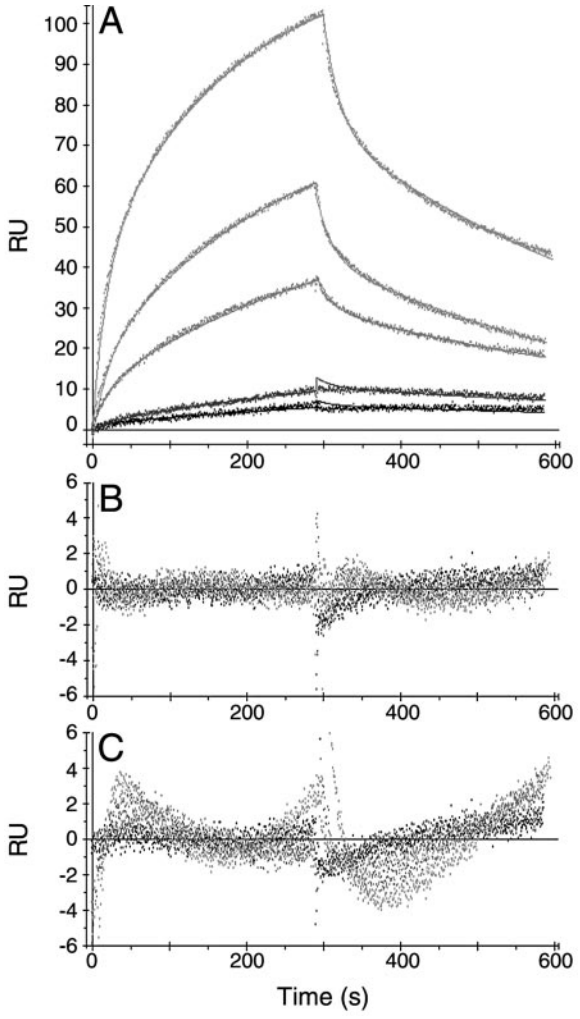

FIG. 3. **Global analysis of the type III ED interaction with the TGF-β3 isoform.** *A*, global fit of the type III ED/TGF-β3 interaction sensorgrams. Different concentrations of the type III ED ranging from 50 to 800 nM were injected over 350 RU of immobilized TGF-β3 and over a control dextran surface. The *points* are the resonance units obtained after blank subtraction, and the *solid lines* represent the fit when integrating all the curves simultaneously using a two-sited analyte (avidity) model. *B*, residuals from the fit of the type III ED/TGF-β3 interaction using the two-sited analyte (avidity) model. *C*, residuals from the fit of the type III ED/TGF-β3 interaction using a simple one-to-one model.

ligand, and two-sited binding protein models, when applied to the LAP and type II and III ED interactions, respectively, yielded similar values for the amount of active TGF-β1 on the surface (ranging from 27 to 33 RU). No other combination of models gave a consistent value for the amount of active TGF-β1 on the surface. This further supports the validity of the different kinetic models. Additionally, the kinetic constants determined in this experiment were similar to those determined using the optimized TGF-β1 isoform surfaces (<10% difference) (data not shown).

The stoichiometry of binding for the type II ED/Fc chimera was confirmed by injecting the type II ED/Fc chimera and the type II ED over the same TGF-β1 and TGF-β3 surfaces. The amounts of immobilized active TGFs-β were first calculated by curve fitting the type II ED/Fc chimera sensorgrams using the 1:1 stoichiometry rearrangement model. These numbers were then compared with the amounts of immobilized active TGFs-β determined by saturating the surfaces with the type II ED (injections of 1.5 and 2 μM type II ED solutions were used to confirm that the surfaces were saturated). In all cases, we obtained the same value for the amount of active TGFs-β within a 1-RU difference only when assuming a 1:1 stoichiometry for the type II ED/Fc chimera and a 2:1 stoichiometry for the non-dimerized type II ED/TGF-β interaction.

The thermodynamic and kinetic parameters for each TGF-β-binding protein/TGF-β isoform interaction, calculated using the relevant kinetic model and data from optimized surfaces (Figs. 1–4 for TGF-β3 and data not shown for TGF-β1 and TGF-β2), are presented in Tables IV–VII.

Analysis of the Ability of LAP and the Type II and III EDs to Block Subsequent Binding of the Type II or III ED—To use the BIAcore to determine if these three binding proteins interact with TGF-β in independent, competitive, or cooperative manners, we investigated the effect of pre-binding these three proteins to immobilized TGF-β on the subsequent binding of the type II and III receptor ectodomains. The influence of LAP binding on the subsequent binding of the type II and III EDs to TGF-β was relatively straightforward to investigate since LAP has a slow dissociation rate (see Fig. 1*A*). In other words, enough LAP will remain bound during a subsequent injection so that its effect on type II or III ED binding will be detectable. Specifically, injections of LAP at different concentrations were followed by a short buffer injection and then an injection of the type II or III ED at a fixed concentration (400 and 600 nM, respectively). For TGF-β1 and TGF-β3 isoform surfaces, type II

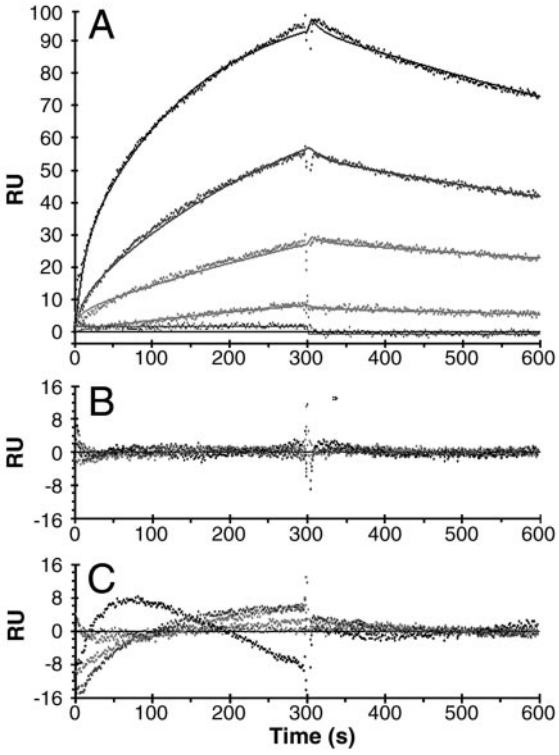

FIG. 4. **Global analysis of the type II ED/Fc chimera interaction with the TGF-β3 isoform.** *A*, global fit of the type II ED/Fc chimera/TGF-β3 interaction sensorgrams. Different concentrations of the type II ED/Fc chimera ranging from 18 to 500 nM were injected over 240 RU of immobilized TGF-β3 and over a control dextran surface. The *points* are the resonance units obtained after blank subtraction, and the *solid lines* represent the fit when integrating all the curves simultaneously using a rearrangement model. *B*, residuals from the fit of the type II ED/Fc chimera/TGF-β3 interaction using the rearrangement model. *C*, residuals from the fit of the type II ED/Fc chimera/TGF-β3 interaction using a simple one-to-one model.

ED binding was reduced in a dose-dependent manner by pre-binding increasing amounts of LAP (Fig. 6, *A* and *B*). Since the type II ED does not detectably bind to TGF-β2, this experiment was not done on that isoform surface. Comparable results were obtained when LAP was bound to the three TGF-β isoforms prior to the binding of the type III ED (Fig. 6*C*). That is, LAP inhibited subsequent binding of the type III ED to all TGF-β isoforms in a dose-dependent manner.

Since the dissociation of the type III ED from the TGF-β isoform surfaces is faster than the dissociation of LAP (compare Figs. 1 and 3), we could not use exactly the same experimental strategy to examine its influence on subsequent type II ED binding events. A different type of experiment was performed in which type III ED injections (at various concentrations) were followed immediately by injections containing the type III ED (at the same concentration as in the first injection) together with the type II ED at a fixed concentration. In this way, the dynamics of binding and dissociation of TGF-β with the type III ED were maintained, and it was possible to monitor any perturbation of type II ED binding to TGF-β1 or TGF-β3 caused by the presence of the type III ED. As shown in Fig. 6*D*, both ectodomains could bind simultaneously to TGF-β, and the binding of one did not hinder the binding of the other. The same experiment was conducted over the TGF-β2 surface. Due to the ability of the type III receptor to enhance TGF-β2 binding to the type II receptor at the cell surface (9, 10), it might be expected that the type II and III EDs would exhibit cooperative binding to TGF-β2 on the BIAcore. In the presence of the type III ED, the type II ED still did not exhibit any detectable binding to TGF-β2 (Fig. 6*E*). Reverse experiments examining the influence of type II ED pre-binding on the subsequent binding of the type III ED to TGF-β1 and TGF-β3 were also carried out. As expected from the previous set of experiments, type II ED binding neither blocked nor enhanced subsequent type III ED binding (data not shown).

Ability of LAP, the Type II ED, the Type II ED/Fc chimera, and the Type III ED to Antagonize TGF-β Receptor Signaling—The ability of LAP, the type II ED, the type II ED/Fc chimera, and the type III ED to block TGF-β interactions with cell-surface receptors and subsequent signaling was tested with mink lung epithelial cells stably transfected with a luciferase reporter gene. As shown in Fig. 7*A*, LAP was able to inhibit TGF-β-induced receptor signaling for the three TGF-β isoforms. LAP inhibited receptor signaling by 50% at a 10-fold lower concentration for TGF-β3 as compared with TGF-β1 and TGF-β2 (the IC_{50} was ~1 nM for TGF-β3 *versus* 10 nM for TGF-β1 and TGF-β2). Similar to LAP, the type III ED also exerted an inhibitory effect on TGF-β-induced signaling for all three TGF-β isoforms (Fig. 7*B*). However, the IC_{50} for the type III ED inhibitory effect was found to be ~5 nM for the TGF-β2 and TGF-β3 isoforms, whereas an IC_{50} of ~50 nM was observed in the case of the TGF-β1 isoform. No significant blocking activity was observed with the type II ED up to a concentration of 500 nM (Fig. 7*C*) for all three TGF-β isoforms. In contrast, the artificially dimerized type II ED/Fc chimera exhibited an inhibitory effect with an IC_{50} of ~100 pM for the TGF-β1 and TGF-β3 isoforms (Fig. 7*D*).

DISCUSSION

To study the interaction between TGF-β and four binding proteins (LAP, type II ED, type II ED/Fc chimera and type III ED) using the BIAcore, we immobilized three TGF-β isoforms individually on sensor chips and injected the four binding proteins over the surfaces. This immobilization strategy was chosen since injected TGF-β interacted nonspecifically with a control surface. Our preliminary kinetic analysis revealed that, as observed for many systems studied with the BIAcore, these binding protein/TGF-β interactions failed to be represented as a simple one-to-one interaction. This type of deviation from pseudo first-order kinetics may be explained by artifacts related to less than optimal experimental design (19, 24, 27). On the other hand, these deviations may be explained by the occurrence of more complex interaction mechanisms. After optimizing the experimental design and still observing deviations from a simple kinetic model for the four binding proteins, we tested more complex interaction models by globally fitting the data (*i.e.* all the curves are fit at the same time). This technique has been shown to be the best for discriminating between different complex binding mechanisms (26, 28) and for determining the related kinetic constants (27).

For all three TGF-β isoforms, the LAP binding data were best fit by a model depicting a one-to-one interaction, followed by a rearrangement of the LAP·TGF-β complex (Fig. 1). Type II ED interactions with TGF-β1 and TGF-β3 isoforms were best described by a model assuming that TGF-β possesses two independent binding sites for the type II receptor (Fig. 2). Consistent with a preliminary study performed in our laboratory (29), we could not detect any interaction between the type II ED and the TGF-β2 isoform, even when high amounts of TGF-β2 were immobilized. The type III ED interaction data were best fit with an avidity model, which depicts the presence of two independent binding sites on the type III ED, with these sites being able to bind sequentially to two immobilized TGF-β molecules (Fig. 3). Finally, the type II ED/Fc chimera binding data were best fit, as with LAP, by the 1:1 stoichiometry rearrangement model (Fig. 4). These different stoichiometries of binding

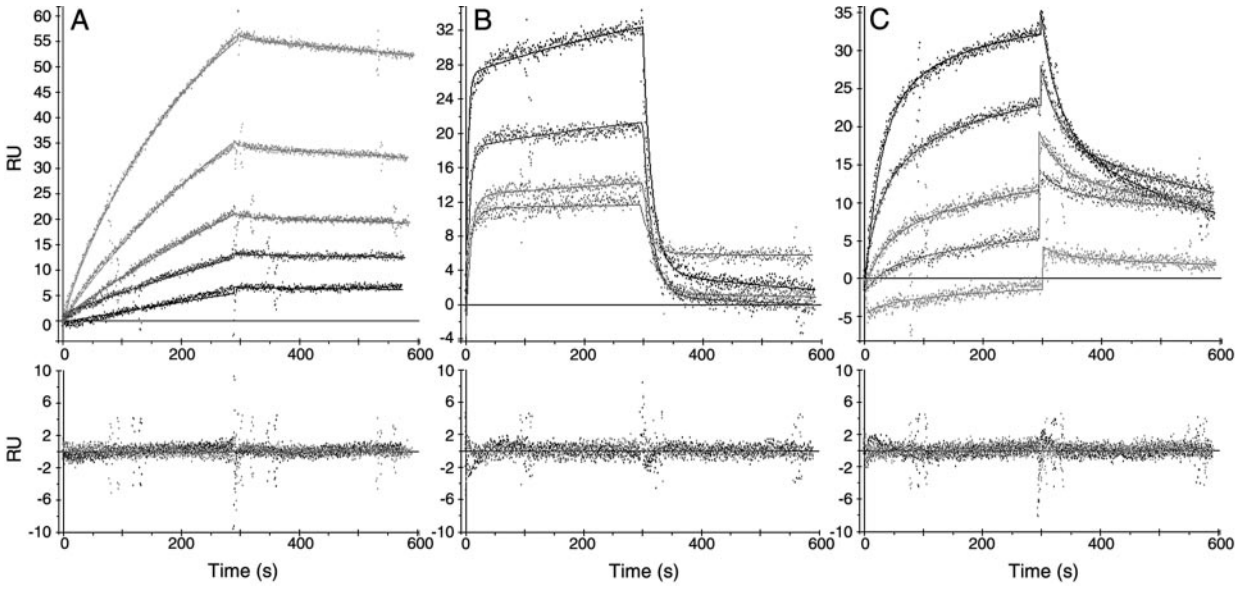

FIG. 5. **Global analysis of the LAP and type II and III ED interactions with the TGF-β1 isoform on the same surface.** *A*: *upper panel*, different concentrations of LAP ranging from 25 to 400 nM were injected over 125 RU of immobilized TGF-β1 and over a control dextran surface. The *points* are the resonance units obtained after blank subtraction, and the *solid lines* represent the fit when integrating all the curves simultaneously using a rearrangement model. *Lower panel*, shown are the related residuals. *B*: *upper panel*, different concentrations of the type II ED ranging from 25 to 400 nM were injected over the same surfaces as described for *A*. The *points* are the resonance units obtained after blank subtraction, and the *solid lines* represent the fit when integrating all the curves simultaneously using a two-sited ligand model. *Lower panel*, shown are the related residuals. *C*: *upper panel*, different concentrations of the type III ED ranging from 37.5 to 600 nM were injected over the same surfaces as described for *A*. The *points* are the resonance units obtained after blank subtraction, and the *solid lines* represent the fit when integrating all the curves simultaneously using a two-sited analyte (avidity) model. *Lower panel*, shown are the related residuals.

TABLE III
Quantity of active immobilized TGF-β1 as determined by numerical analysis of the LAP, type II ED, and type III ED/TGF-β1 sensorgrams shown in Fig. 5

The best combination of models is shown in boldface type.

Kinetic model used	LAP	Type II ED	Type III ED
	RU	*RU*	*RU*
Rearrangement of complex	**28.3 ± 0.5**	43.0 ± 1.2	15.4 ± 0.4
Two sites on ligand	21.5 ± 3.5	**33.0 ± 1.0**	7.5 ± 0.2
Two sites on analyte (avidity)	65.3 ± 3.6	13.1 ± 1.5	**27.0 ± 0.8**

and kinetic models were confirmed by carrying out internal consistency tests in which these TGF-β-binding proteins were injected over the same TGF-β surfaces (Fig. 5 and Table III).

The LAP interaction with the TGF-β1 isoform has previously been studied on the BIAcore by Bailly *et al.* (30). They were able to fit the sensorgrams with a simple one-to-one model by analyzing the data using the integrated rate equation method. Global analysis of the data was not performed since the software tools for this type of analysis were not generally available at that time. Our results are in agreement with theirs in that our best fitting model depicts a 1:1 stoichiometry for the LAP/TGF-β interaction not only for TGF-β1, but also for TGF-β2 and TGF-β3. However, the global fit of the data revealed a second step involving a rearrangement of the complex. The 1:1 stoichiometry for the LAP/TGF-β interaction is not unexpected since LAP is the remnant of the precursor form of TGF-β. Accordingly, during biosynthesis, LAP and TGF-β would be associated as a one-to-one complex. The finding that this complex undergoes a rearrangement can be interpreted in two ways. Since both TGF-β and LAP are covalent dimers, it can be proposed that the first step in complex formation involves the interaction between one monomer of each of LAP and TGF-β and that the rearranged complex corresponds to a complex in which both monomers of LAP and TGF-β are interacting. This second binding step would have zero order kinetics since it occurs intramolecularly. Alternatively, the rearrangement step may correspond to a conformational change in the complex. This latter mechanism is supported by far-UV circular dichroism studies performed by McMahon *et al.* (31), who showed that the LAP·TGF-β complex undergoes a major structural rearrangement after binding. We also recently found that BIAcore data for the interaction of TGF-α with the epidermal growth factor receptor extracellular domain could be fit with a conformational change model (28). In this case, the model was also supported by far-UV circular dichroism studies (32). A comparison of the apparent thermodynamic K_d values (defined as $K_{d(app)}$ = ([LAP] × [TGF-β])/([LAP·TGF-β] + [LAP·TGF-β rearranged])) (Table IV) for the LAP interaction with the three TGF-β isoforms reveals that the affinity of LAP for each TGF-β isoform is very similar and in the low nanomolar range. This is in close agreement with the value estimated by Bailly *et al.* (30) for the LAP/TGF-β1 interaction using a simple model. This relatively high affinity for the LAP/TGF-β interaction results primarily from a relatively slow k_{d2} dissociation rate (3–5 × 10^{-4} s^{-1}) (Fig. 1 and Table IV).

In the case of the type II ED interaction with TGF-β1 and TGF-β3, the finding that the best fitting model involves a stoichiometry of two receptors for one ligand is consistent with the dimeric and symmetrical nature of the TGF-β molecule (33–35). Moreover, Matsuzaki *et al.* (36) also reported the formation of a type II receptor homodimer that complexes one TGF-β1 molecule by expressing full-length recombinant receptors in insect cells. Additionally, it has been shown in *in vitro* experiments that the stoichiometry of binding of the type II ED to the TGF-β3 isoform is 2:1 (37). Somewhat surprisingly in light of the symmetric nature of the TGF-β structure, we found that the thermodynamic K_d values determined for each type II ED-binding site within the TGF-β dimer differ by 5–7-fold, depending on the TGF-β isoform (Table V). This affinity difference may be the result of the coupling procedure we used to immobilize TGF-β. That is, amine coupling may have gener-

TABLE IV
Kinetic and thermodynamic constants for TGF-β isoforms interacting with LAP

All the notations for the constants used below are consistent with the ones used in Table I.

Kinetic parameters	Kinetic model: rearrangement of complex		
	TGF-β1 isoform	TGF-β2 isoform	TGF-β3 isoform
k_{a1} (M^{-1} s^{-1})	$(1.7 \pm 0.3) \times 10^4$	$(4.3 \pm 0.2) \times 10^4$	$(1.22 \pm 0.04) \times 10^5$
k_{d1} (s^{-1})	$(3.4 \pm 1.5) \times 10^{-2}$	$(2.4 \pm 0.2) \times 10^{-2}$	$(1.9 \pm 0.1) \times 10^{-2}$
k_{a2} (s^{-1})	$(4.9 \pm 0.9) \times 10^{-2}$	$(1.55 \pm 0.06) \times 10^{-2}$	$(1.34 \pm 0.06) \times 10^{-2}$
k_{d2} (s^{-1})	$(4.9 \pm 0.1) \times 10^{-4}$	$(2.3 \pm 0.2) \times 10^{-4}$	$(2.9 \pm 0.2) \times 10^{-4}$
K_{d1} (nM)[a]	1900 ± 1200	560 ± 70	150 ± 100
K_{d2} (no unit)	$(1.0 \pm 0.4) \times 10^{-2}$	$(1.5 \pm 0.2) \times 10^{-2}$	$(2.1 \pm 0.3) \times 10^{-2}$
$K_{d(app)}$ (nM)[b]	23.5 ± 3.5 ($n = 2$)	6.6 ± 2.5 ($n = 5$)	3.5 ± 1.1 ($n = 3$)

[a] K_{d1} corresponds to the thermodynamic constant related to the first binding step (see Table I for the description of the model). $K_{d1} = ([L] \times [A]/[LA] = k_{d1}/k_{a1}$.

[b] K is defined as $K_{d(app)} = 1/K_{a(app)}$ where $K_{a(app)} = K_{a1} \times (1 + K_{a2})$ with $K_{a1} = k_{a1}/k_{d1}$ and $K_{a2} = k_{a2}/k_{d2} \cdot K_{d(app)}$ corresponds to the global thermodynamic constant related to the interaction since $K_{d(app)} = ([L] \times [A])/([LA] + [LA^*])$. The values given for $K_{d(app)}$ correspond to the mean ± S.D. of n independent experiments.

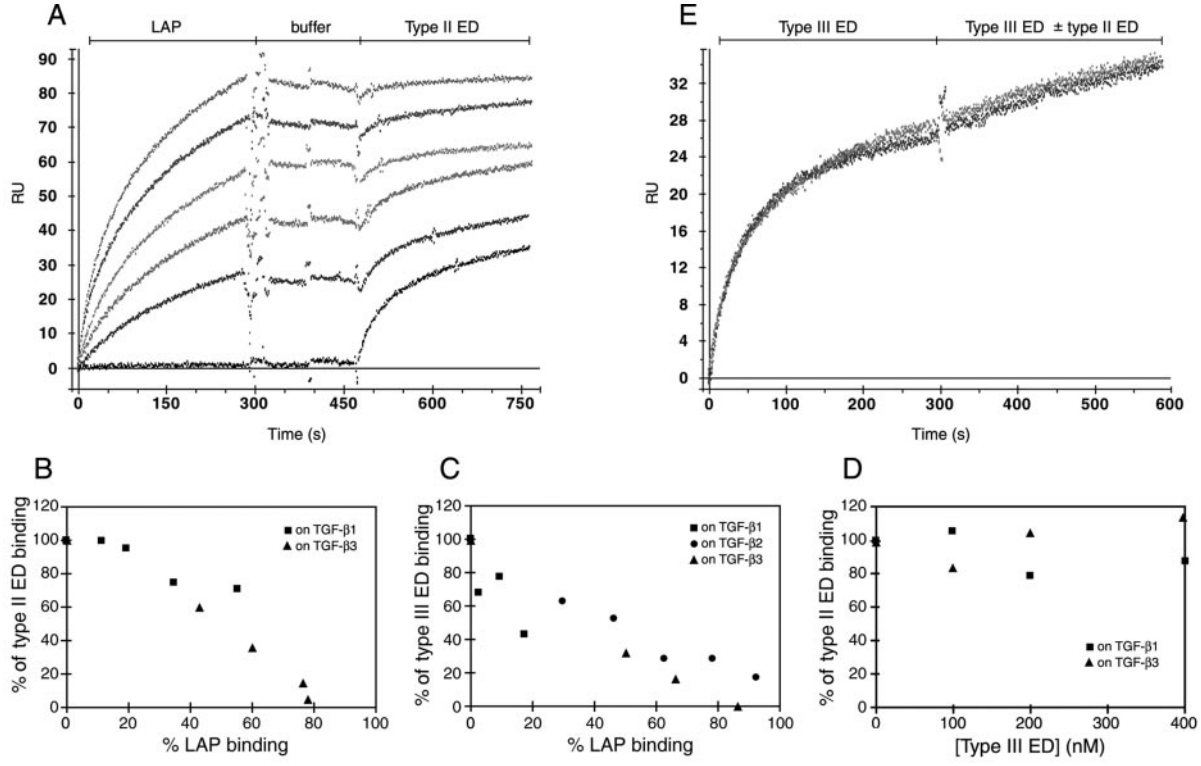

FIG. 6. **Analysis of the ability of LAP and the type II and III EDs to block the subsequent binding of type II or III ED.** *A*, example of the effect of LAP pre-binding on the subsequent binding of the type II ED to TGF-β3. 300-s injections of LAP (ranging in concentration from 0 to 400 nM) were performed over TGF-β3 (250 RU) and control dextran surfaces. All injections were followed by a short wash-off phase and a 300-s injection of 400 nM type II ED. *B*, effect of LAP pre-binding on the subsequent type II ED binding to the TGF-β1 and TGF-β3 isoforms. Results from *A* and similar experiments conducted with the TGF-β1 isoform were analyzed and plotted as described under "Experimental Procedures." The *y axis* corresponds to the amount of type II ED bound at the end of the type II ED injection and is expressed as a percentage of type II ED binding in the absence of LAP pre-binding. The *x axis* corresponds to the amount of LAP that was pre-bound at the end of the LAP injection and is expressed as a percentage of maximum LAP binding for that surface. Maximum LAP binding was determined by integrating numerically the sensorgrams using a rearrangement model. *C*, effect of LAP pre-binding on subsequent type III ED binding to the three TGF-β isoforms. Similar experiments were conducted with the type III ED and plotted as with the type II ED (see "Experimental Procedures"). *D*, effect of type III ED on type II ED binding to the TGF-β1 and TGF-β3 isoforms. Injections of the type III ED (0–800 nM) were immediately followed by co-injection of a mixture of the type III ED (at the same concentration) and the type II ED at 500 nM. The results are expressed as a percentage of type II ED binding in the absence of the type III ED and are plotted against the concentration of type III ED injected. *E*, effect of type III ED binding on type II ED binding to the TGF-β2 isoform. Injection of the type III ED (800 nM) followed by injection of a type III ED (800 nM)/type II ED (400 nM) mixture over a TGF-β2 surface gave a sensorgram that was similar to the one corresponding to the injection of the type III ED (800 nM) alone.

ated asymmetry in the immobilized TGF-β, thereby reducing the affinity of one of the two sites. Even though amine coupling may have somewhat affected the affinity of one site within the TGF-β dimer, it is unlikely that the stoichiometry of TGF-β1 and TGF-β3 binding to type II ED has been perturbed. With this proposed immobilization effect in mind, it can be concluded that the equilibrium K_d for the high affinity site is likely to be the most relevant. This K_d was determined to be in the 100 nM range for both the TGF-β1 and TGF-β3 isoforms, and it results from k_a values of $\sim 6 \times 10^5$ M^{-1} s^{-1} and k_d values of $\sim 6 \times 10^{-2}$ s^{-1} (Table V).

In the case of the type II ED/Fc chimera, the model found to best depict the interaction was a one-to-one interaction, followed by a rearrangement of the complex. The apparent K_d values were found to be equal to 60 and 50 nM for TGF-β1 and TGF-β3, respectively (see Table VII). The change in the stoichiometry between the type II ED/Fc chimera model and the type II ED model is not surprising in that the artificial dimer-

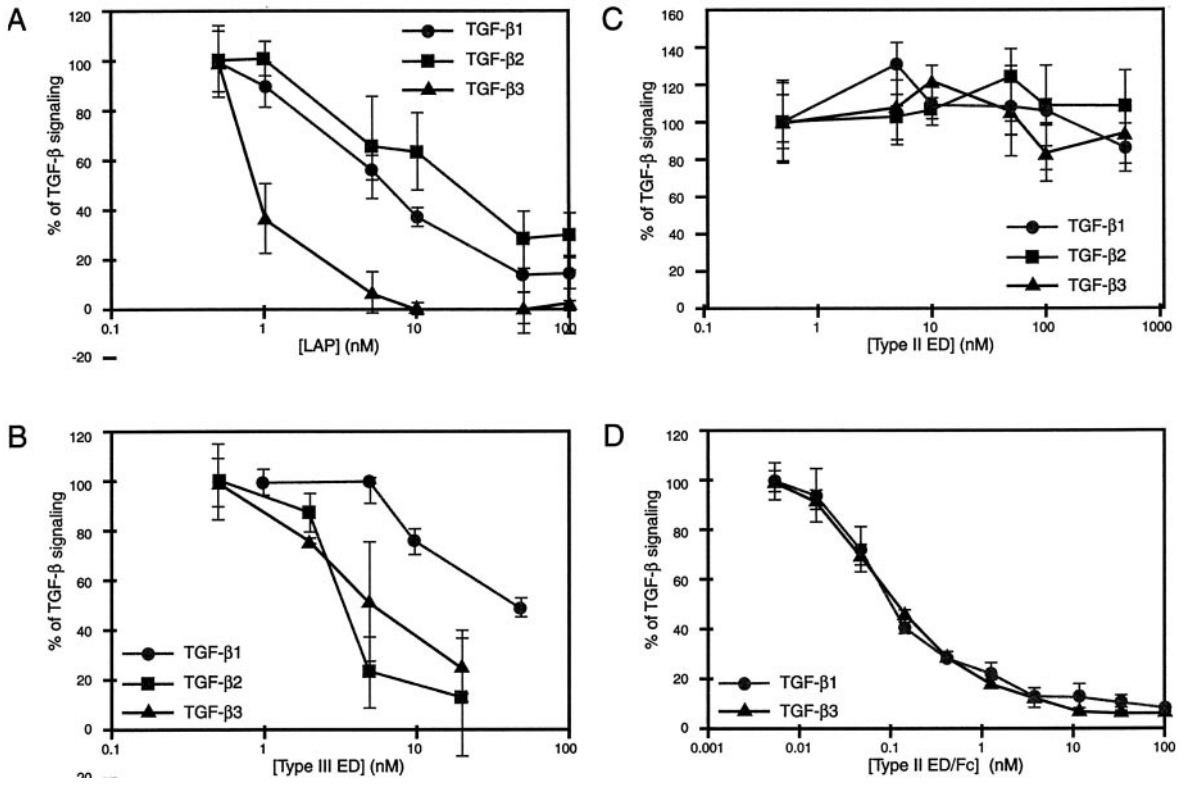

FIG. 7. **Evaluation of the antagonistic potency of LAP, the type II and III EDs, and the type II ED/Fc chimera using a TGF-β-responsive luciferase reporter assay in mink lung epithelial cells.** The cells were incubated with TGF-β isoforms in the absence or presence of varying concentrations of LAP (*A*), the type III ED (*B*), the type II ED (*C*), and the type II ED/Fc chimera (*D*), and the luciferase activity was assayed as described under "Experimental Procedures."

TABLE V
Kinetic and thermodynamic constants for TGF-β isoforms interacting with the type II ED

All the notations for the constants used below are consistent with the ones used in Table I. The values given for K_{d1} and K_{d2} correspond to the mean ± S.D. of n independent experiments.

Kinetic parameters	Kinetic model: two sites on TGF-β		
	TGF-β1 isoform	TGF-β2 isoform	TGF-β3 isoform
k_{a1} (M^{-1} s^{-1})	$(5.4 \pm 0.3) \times 10^5$		$(6.1 \pm 0.1) \times 10^5$
k_{d1} (s^{-1})	$(6.5 \pm 0.2) \times 10^{-2}$		$(4.8 \pm 0.07) \times 10^{-2}$
k_{a2} (M^{-1} s^{-1})	$(1.8 \pm 0.1) \times 10^3$		$(2.5 \pm 0.1) \times 10^4$
k_{d2} (s^{-1})	$(1.5 \pm 0.3) \times 10^{-3}$	No binding	$(9.8 \pm 0.2) \times 10^{-4}$
K_{d1} (nM)	158 ± 37 (n = 6)		150 ± 100 (n = 3)
K_{d2} (nM)	981 ± 123 (n = 6)		294 ± 166 (n = 3)

ization of the type II ED that is induced by fusion to the Fc domain might be expected to convert the type II ED/TGF-β interaction model from a 2:1 monomeric receptor/dimeric ligand stoichiometry model into a 1:1 dimeric receptor/dimeric ligand model. It is likely then that the first step in the formation of the type II ED/Fc chimera·TGF-β complex involves the interaction between one monomer of each of the proteins and that the rearranged complex has both monomers within each dimer interacting.

Mutational studies have shown that the type III ED has two binding sites for TGF-β that are located in the N- and C-terminal regions of the ectodomain (11, 12, 15, 38). However, the stoichiometry of binding to TGF-β remains unclear. Indeed, one can envision the type III receptor as having two binding sites, with each one binding a dimeric molecule of TGF-β, or as having two binding sites, with each one interacting with a TGF-β monomer such that the dimeric molecule of TGF-β bridges the two binding sites. Our current results support the first hypothesis: global analysis of the type III ED sensorgrams were best fit by a kinetic model depicting the presence of two independent TGF-β-binding sites on the type III ED (Tables II and III). Despite the good quality of the fit when using this two-sited receptor model (avidity), the calculated kinetic and equilibrium constants (Table VI) must be considered with great care, as emphasized by Muller *et al.* (39). They showed that kinetic constants that are derived with an avidity model are difficult to interpret in meaningful terms, even in the simpler case of a bivalent antibody where the two sites are equal. However, they also concluded that the avidity model is still relevant for distinguishing among different kinetic models. Since the constants determined using the avidity model and global fitting (Table VI) must be interpreted with caution, we also estimated the apparent thermodynamic K_d values for the type III ED/TGF-β isoform interactions using the plateau values from the sensorgrams in Scatchard plots (data not shown). These calculations estimated the equilibrium K_d values to range between 300 and 1000 nM. It must be emphasized that these numbers are approximate since the plateaus were only being approached in some of the sensorgrams.

To determine if LAP and the type II and III EDs bind to TGF-β in independent, competitive, or cooperative manners, we studied, using the BIAcore, if the binding of one of these three proteins to TGF-β would alter the subsequent binding of the type II or III ED. When varying concentrations of LAP were injected prior to the type II or III ED, we observed a dose-dependent decrease in the binding of both ectodomains (Fig. 6, *A–C*). These results indicate that LAP binding to TGF-β inhibits its binding to three receptor sites: one on the type II ED and two on the type III ED. The conformational change model for the LAP/TGF-β interaction may provide a simple explanation for this result if one assumes that the conformational change occurs in the TGF-β moiety within the complex. In other words, a conformational change could readily affect several binding sites within the TGF-β ligand. We cannot exclude, however,

TABLE VI

Kinetic and thermodynamic constants for TGF-β isoforms interacting with the type III ED

All the notations used below are consistent with the ones used in Table I. The values given for K_{d1} and K_{d2} correspond to the mean ± S.D. of n independent experiments.

Kinetic parameters	Kinetic model: Two sites on type III ED		
	TGF-β1 isoform	TGF-β2 isoform	TGF-β3 isoform
k_{a1} (M^{-1} s^{-1})	$(1.4 \pm 0.4) \times 10^4$	$(1.6 \pm 0.4) \times 10^4$	$(1.7 \pm 0.2) \times 10^3$
k_{d1} (s^{-1})	$(2.9 \pm 0.1) \times 10^{-2}$	$(4.0 \pm 0.2) \times 10^{-2}$	$(1.0 \pm 0.2) \times 10^{-2}$
k_{a2} (M^{-1} s^{-1})	$(6.8 \pm 0.4) \times 10^2$	$(1.7 \pm 0.07) \times 10^3$	$(0.7 \pm 0.1) \times 10^3$
k_{d2} (s^{-1})	$(3.5 \pm 0.2) \times 10^{-3}$	$(2.6 \pm 0.06) \times 10^{-3}$	$(2.2 \pm 0.3) \times 10^{-3}$
K_{d1} (nM)	2074 ± 500 (n = 3)	2500 ± 50 (n = 3)	4560 ± 1500 (n = 3)
K_{d2} (nM)	4274 ± 1340 (n = 3)	2173 ± 800 (n = 3)	3990 ± 1200 (n = 3)

TABLE VII

Kinetic and thermodynamic constants for TGF-β isoforms interacting with the type II ED/Fc chimera

All the notations for the constants used below are consistent with the ones used in Table I.

Kinetic parameters	Kinetic model: rearrangement of the complex		
	TGF-β1 isoform	TGF-β2 isoform	TGF-β3 isoform
k_{a1} (M^{-1} s^{-1})	$(5.3 \pm 0.3) \times 10^4$		$(4.6 \pm 0.3) \times 10^4$
K_{d1} (s^{-1})	$(2.7 \pm 0.2) \times 10^{-2}$		$(5.2 \pm 0.5) \times 10^{-2}$
k_{a2} (s^{-1})	$(9.4 \pm 0.4) \times 10^{-3}$		$(2.3 \pm 0.1) \times 10^{-2}$
k_{d2} (s^{-1})	$(1.26 \pm 0.05) \times 10^{-3}$	No binding	$(1.30 \pm 0.04) \times 10^{-3}$
K_{d1} (nM)[a]	509 ± 71		1126 ± 193
K_{d2} (no unit)	$(1.35 \pm 0.01) \times 10^{-1}$		$(5.7 \pm 0.4) \times 10^{-2}$
$K_{d(app)}$ (nM)[b]	60 ± 10 (n = 3)		50.5 ± 14 (n = 3)

[a] K_{d1} corresponds to the thermodynamic constant related to the first binding step (see Table I for the description of the model). $K_{d1} = ([L] \times [A]/[LA]) = k_{d1}/k_{a1}$.

[b] $K_{d(app)}$ is defined as $K_{a(app)} = 1/K_{a(app)}$ where $K_{a(app)} = K_{a1} \times (1 + K_{a2})$ with $K_{a1} = k_{a1}/k_{d1}$ and $K_{a2} = k_{a2}/k_{d2}$. $K_{d(app)}$ corresponds to the global thermodynamic constant related to the interaction since $K_{d(app)} = ([L] \times [A])/([LA] + [LA^*])$. The values given for $K_{d(app)}$ correspond to the mean ± S.D. of n independent experiments.

that LAP binds to TGF-β in such a way that it sterically blocks binding to the type II ED and both sites on the type III ED.

In contrast, in these BIAcore multiple binding experiments, type II and III EDs were found to bind to TGF-β1 and TGF-β3 in an independent fashion since the pre-binding of one did not affect the subsequent binding of the other (Fig. 6*D* and data not shown). This indicates that the binding sites on TGF-β for these two extracellular domains are distinct and non-cooperative. Additionally, type III ED pre-binding to TGF-β2 was not able to promote type II ED binding to the TGF-β2 isoform (Fig. 6*E*), as might have been expected from the observation that the type III receptor is able to enhance TGF-β2 binding to the type II receptor at the cell surface (9, 10). These results suggest that the extracellular domains of the type II and III receptors are not sufficient to mimic the type III receptor-enhanced binding of TGF-β2 to the type II receptor and that the transmembrane and/or cytoplasmic domains must be involved in this process. This conclusion is supported by our data showing that the cytoplasmic domains of the type II and III receptors interact such that an antibody epitope on the type III receptor cytoplasmic domain is masked by the presence of the type II receptor (41).

These BIAcore experiments were complemented by a luciferase reporter assay in mink lung epithelial cells, which was used to evaluate the antagonistic potency of LAP, the type II ED, the type II ED/Fc chimera, and the type III ED (Fig. 7). LAP was found to inhibit TGF-β signaling for all three TGF-β isoforms with IC_{50} values of ~1 nM for TGF-β3 and ~10 nM for TGF-β1 and TGF-β2. Similar to LAP, the type III ED also inhibited signaling for all three TGF-β isoforms. However, the IC_{50} values were ~50 nM for TGF-β1 and ~5 nM for TGF-β2 and TGF-β3. No inhibition of signaling was observed at any type II ED concentration up to 500 nM. In contrast, the type II ED/Fc chimera was found to be the best antagonist for TGF-β1 and TGF-β3 with an IC_{50} of 100 pM for both isoforms. Our results on the neutralizing potency of the type II ED and the type II ED/Fc chimera are similar to those of Komesli *et al.* (40) for TGF-β1.

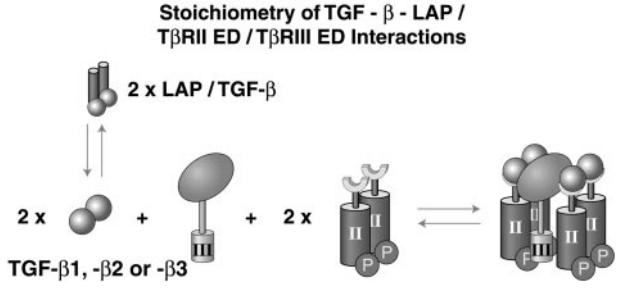

FIG. 8. **Proposed model for TGF-β binding to cell-surface receptors.** Based on the different stoichiometries of binding determined for the TGF-β-binding protein/TGF-β interactions, we propose that the cell-surface receptor·ligand complex is composed of one type III receptor, two TGF-β ligands, and four type II receptors. Additionally, LAP is able to bind to the three TGF-β isoforms with a 1:1 stoichiometry and compete for their interaction with the cell-surface receptors (see "Discussion" for details). *TβRII ED*, TGF-β type II receptor ED.

The striking difference in the abilities of the type II ED *versus* the type II ED/Fc chimera to sequester TGF-β and thus inhibit signaling (Fig. 7, *C* and *D*) can be directly correlated with their apparent dissociation rates (compare the wash-off phases in Figs. 2 and 4 and k_{d1} from Table V with k_{d2} from Table VII), but not with their thermodynamic dissociation constants (~100 nM) (see Tables V and VII). These results indicate that the apparent dissociation rate, and not the thermodynamic dissociation constant, may be the parameter that best explains the antagonistic potential of a TGF-β-binding protein. In the case of the type II ED/Fc chimera, the decrease in the apparent off-rate is likely due to an effect that appears as a rearrangement of the complex (*i.e.* the complex with two sites interacting rearranges to a complex with one site interacting; the slow off-rate is reflected in a slow k_{d2} in Table VII).

With respect to the antagonistic potency of the type III ED and LAP, we propose that, as for the type II ED and the type II ED/Fc chimera, their potency can be explained, at least in part, by their apparent dissociation rate. That is, we are suggesting

that they neutralize TGF-β relatively effectively (in the 1–100 nM range depending on the binding protein/TGF-β isoform combination) (Fig. 7, *A* and *B*) due to the fact that they have relatively slow apparent dissociation rates (compare wash-off phases in Fig. 1–4). In the case of LAP, these slow apparent dissociation rates are reflected in the k_{d2} dissociation constants (Table IV) and are visually obvious (Fig. 1). In the case of the type III ED, as discussed above, the values of the constants derived from the avidity model are difficult to interpret; however, a visual evaluation of the wash-off phase for the type III ED/TGF-β interaction (Fig. 3) illustrates that it is biphasic, with an obviously slow component. The fact that the type III ED antagonizes as well as it does could be considered surprising due to the fact that the type II and III EDs bind to TGF-β in a non-competitive manner (Fig. 6, *D* and *E*), *i.e.* the type III ED-bound ligand should still be able to bind to cell-surface type II receptors. The antagonistic potency of the type III ED may be explained by our data showing that an interaction between the cytoplasmic domains of the type II and III receptors is critical for enhancement of TGF-β signaling (41). Together, these results suggest an active role for the type III receptor in signaling in addition to concentrating TGF-β at the cell surface.

The above discussion suggests that the dissociation rate may be used to explain the antagonistic potency. However, in the case where the dissociation rate is held constant, as occurs when comparing the LAP interaction with the three TGF-β isoforms (k_{d2} varies <2-fold depending on the isoform) (Table IV), it becomes apparent that the association rate (k_a) also has to be taken into consideration. A comparison of the on-rates for LAP interacting with the three TGF-β isoforms reveals that LAP interacts with TGF-β3 with a 3–10-fold faster k_{a1} compared with TGF-β1 and TGF-β2 (Table IV). The variation in this kinetic constant correlates with the variation in the antagonistic potency of LAP for the three isoforms, *i.e.* LAP neutralizes TGF-β3 more effectively than the two other isoforms (Fig. 7*A*). Hence, although kinetic parameters are explanatory, no single kinetic parameter correlates with antagonistic potency in all cases.

In addition to providing an explanation for the antagonistic potency of soluble TGF-β-binding proteins, the BIAcore data also enable us to construct a model of the cell-surface ligand-occupied TGF-β receptor complex. Based on the stoichiometry of binding that was determined using the BIAcore, we propose that the cell-surface receptor·ligand complex is composed of one type III receptor, two TGF-β ligands, and four type II receptors (Fig. 8). It is likely that this complex recruits four type I receptors based on the recently reported structure of bone morphogenetic protein-2 in complex with two bone morphogenetic protein type IA receptor extracellular domains (42). One of the most salient features of this model relative to ones suggested previously (36) is that the type III receptor is proposed to induce the formation of a higher order complex of type I and II receptors. In other words, without the type III receptor, the complex would consist of one ligand and two type II and two type I receptors. In the presence of the type III receptor, the number of ligand and type I and II receptor molecules that are held in close proximity would double. This model suggests that the type III receptor plays an important role not only in concentrating ligand at the cell surface, as has been previously suggested, but also in assembling a potentially more productive type I receptor·type II receptor·ligand complex. This may explain the finding that the responsiveness of certain cells to exogenous TGF-β1 depends entirely on the presence of the type III receptor (43). Also, the type III receptor has been shown to have an essential role in mediating the effects of TGF-β on mesenchymal transformation in chick embryonic heart development (44). Additionally, we have recently shown that the type III receptor cooperates in the down-regulation of the type I receptor·type II receptor·TGF-β complex (45), again pointing to an important role for the type III receptor in the formation of the type I receptor·type II receptor·ligand complex.

In summary, we have shown that BIAcore data can be used to derive kinetic constants that can explain the antagonistic potency of soluble TGF-β-binding proteins and to determine stoichiometries that allow the construction of a revised model for the cell-surface ligand-occupied TGF-β receptor signaling complex.

Acknowledgments—We thank Drs. D. D. Mousseau and A. E. G. Lenferink for insightful comments during the preparation of the manuscript.

REFERENCES

1. Wahl, S. M., McCartney-Francis, N., and Mergenhagen, S. E. (1989) *Immunol. Today* **10,** 258–261
2. Massague, J. (1990) *Annu. Rev. Cell Biol.* **6,** 597–641
3. Sporn, M. B., and Roberts, A. B. (1992) *J. Cell Biol.* **119,** 1017–1021
4. Massague, J., Blain, S. W., and Lo, R. S. (2000) *Cell* **103,** 295–309
5. Gentry, L. E., and Nash, B. W. (1990) *Biochemistry* **29,** 6851–6857
6. Wrana, J. L., Attisano, L., Carcamo, J., Zentella, A., Doody, J., Laiho, M., Wang, X. F., and Massague, J. (1992) *Cell* **71,** 1003–1014
7. Padgett, R. W., Das, P., and Krishna, S. (1998) *Bioessays* **20,** 382–390
8. Massague, J. (1998) *Annu. Rev. Biochem.* **67,** 753–791
9. Moustakas, A., Lin, H. Y., Henis, Y. I., Plamondon, J., O'Connor-McCourt, M. D., and Lodish, H. F. (1993) *J. Biol. Chem.* **268,** 22215–22218
10. Lopez-Casillas, F., Wrana, J. L., and Massague, J. (1993) *Cell* **73,** 1435–1444
11. Pepin, M.-C., Beauchemin, M., Plamondon, J., and O'Connor-McCourt, M. D. (1994) *Proc. Natl. Acad. Sci. U. S. A.* **91,** 6997–7001
12. Pepin, M.-C., Beauchemin, M., Collins, C., Plamondon, J., and O'Connor-McCourt, M. D. (1995) *FEBS Lett.* **377,** 368–372
13. Kaname, S., and Ruoslahti, E. (1996) *Biochem. J.* **315,** 815–820
14. Taniguchi, A., Matsuzaki, K., Nakano, K., Kan, M., and McKeehan, W. L. (1998) *In Vitro Cell. Dev. Biol. Anim.* **34,** 232–238
15. Lopez-Casillas, F., Payne, H. M., Andres, J. L., and Massague, J. (1994) *J. Cell Biol.* **124,** 557–568
16. Lin, H. Y., Moustakas, A., Knaus, P., Wells, R. G., Henis, Y. I., and Lodish, H. F. (1995) *J. Biol. Chem.* **270,** 2747–2754
17. Gilboa, L., Wells, R. G., Lodish, H. F., and Henis, Y. I. (1998) *J. Cell Biol.* **140,** 767–777
18. Tsang, M. L., Zhou, L., Zheng, B. L., Wenker, J., Fransen, G., Humphrey, J., Smith, J. M., O'Connor-McCourt, M., Lucas, R., and Weatherbee, J. A. (1995) *Cytokine* **7,** 389–397
19. O'Connor-McCourt, M. D., De Crescenzo, G., Lortie, R., Lenferink, A. E. G., and Grothe, S. (1998) in *Quantitative Analysis of Biospecific Interactions* (Lundqvist, A., and Greijer, E., eds) pp. 175–190, Harwood Academic Publishers GmbH, Chur, Switzerland
20. Press, W. H., Flannery, B. P., Teukolsky, S. A., and Vetterling, W. T. (1986) *Numerical Recipes, the Art of Scientific Computing*, Cambridge University Press, Cambridge
21. Marquardt, D. W. (1963) *J. Soc. Indust. Appl. Math.* **11,** 431–441
22. Bradley, J. V. (1968) *Distribution-Free Statistical Tests*, pp. 251–282, Prentice Hall Inc., Upper Saddle River, NJ
23. Abe, M., Harpel, J. G., Metz, C. N., Nunes, I., Loskutoff, D. J., and Rifkin, D. B. (1994) *Anal. Biochem.* **216,** 276–284
24. O'Shannessy, D. J., and Winzor, D. J. (1996) *Anal. Biochem.* **236,** 275–283
25. Fivash, M., Towler, E. M., and Fisher, R. J. (1998) *Curr. Opin. Biotechnol.* **9,** 97–101
26. Fisher, R. J., and Fivash, M. (1994) *Curr. Opin. Biotechnol.* **5,** 389–395
27. Morton, T. A., Myszka, D. G., and Chaiken, I. M. (1995) *Anal. Biochem.* **227,** 176–185
28. De Crescenzo, G., Grothe, S., Lortie, R., Debanne, M. T., and O'Connor-McCourt, M. (2000) *Biochemistry* **39,** 9466–9476
29. O'Connor-McCourt, M. D., Segarubu, O., Grothe, S., Tsang, M., and Weatherbee, J. A. (1995) *Ann. N. Y. Acad. Sci.* **766,** 300–302
30. Bailly, S., Brand, C., Chambaz, E. M., and Feige, J. J. (1997) *J. Biol. Chem.* **272,** 16329–16334
31. McMahon, G. A., Dignam, J. D., and Gentry, L. E. (1996) *Biochem. J.* **313,** 343–351
32. Greenfield, C., Hiles, I., Waterfield, M. D., Federwisch, M., Wollmer, A., Blundell, T. L., and McDonald, N. (1989) *EMBO J.* **8,** 4115–4123
33. Daopin, S., Piez, K. A., Ogawa, Y., and Davies, D. R. (1992) *Science* **257,** 369–373
34. Mittl, P. R., Priestle, J. P., Cox, D. A., McMaster, G., Cerletti, N., and Grutter, M. G. (1996) *Protein Sci.* **5,** 1261–1271
35. Hinck, A. P., Archer, S. J., Qian, S. W., Roberts, A. B., Sporn, M. B., Weatherbee, J. A., Tsang, M. L., Lucas, R., Zhang, B. L., Wenker, J., and Torchia, D. A. (1996) *Biochemistry* **35,** 8517–8534
36. Matsuzaki, K., Kan, M., and McKeehan, W. L. (1996) *In Vitro Cell. Dev. Biol. Anim.* **32,** 345–360
37. Letourneur, O., Goetschy, J. F., Horisberger, M., and Grutter, M. G. (1996)

Biochem. Biophys. Res. Commun. **224,** 709–716
38. Philip, A., Hannah, R., and O'Connor-McCourt, M. (1999) *Eur. J. Biochem.* **261,** 618–628
39. Muller, K. M., Arndt, K. M., and Pluckthun, A. (1998) *Anal. Biochem.* **261,** 149–158
40. Komesli, S., Vivien, D., and Dutartre, P. (1998) *Eur. J. Biochem.* **254,** 505–513
41. Blobe, G. C., Schiemann, W. P., Pepin, M.-C., Beauchemin, M., Moustakas, A., Lodish, H. F., and O'Connor-McCourt, M. D. (2001) *J. Biol. Chem.* **276,** 24627–24637
42. Kirsch, T., Sebald, W., and Dreyer, M. K. (2000) *Nat. Struct. Biol.* **7,** 492–496
43. Deng, X., Bellis, S., Yan, Z., and Friedman, E. (1999) *Cell Growth Differ.* **10,** 11–18
44. Brown, C. B., Boyer, A. S., Runyan, R. B., and Barnett, J. V. (1999) *Science* **283,** 2080–2082
45. Zwaagstra, J. C., Kassam, Z., and O'Connor-McCourt, M. D. (1999) *Exp. Cell Res.* **252,** 352–362

Real-time Monitoring of the Interactions of Transforming Growth Factor-β (TGF-β) Isoforms with Latency-associated Protein and the Ectodomains of the TGF- β Type II and III Receptors Reveals Different Kinetic Models and Stoichiometries of Binding

Gregory De Crescenzo, Suzanne Grothe, John Zwaagstra, Monica Tsang and Maureen D. O'Connor-McCourt

J. Biol. Chem. 2001, 276:29632-29643.
doi: 10.1074/jbc.M009765200 originally published online May 29, 2001
